JACS
JOURNAL OF THE AMERICAN CHEMICAL SOCIETY
pubs.acs.org/JACS
Article

Directional Construction of Active Naphthalenic Species within SAPO-34 Crystals toward More Efficient Methanol-to-Olefin Conversion

Chang Wang, Liu Yang, Mingbin Gao, Xue Shao, Weili Dai,* Guangjun Wu, Naijia Guan, Zhaochao Xu, Mao Ye, and Landong Li*

Cite This: *J. Am. Chem. Soc.* 2022, 144, 21408−21416
Read Online

ABSTRACT: Olefin selectivity and catalyst lifetime are two key metrics for industrial methanol-to-olefin catalysts. Currently, it is very difficult to obtain high olefin selectivity and long catalyst lifetime at the same time. Herein, a feasible strategy combining precoking and steaming to directionally construct the active naphthalenic species within the crystal center of the SAPO-34 catalyst has been developed, which can not only promote the lower olefin selectivity to ∼89% (ethylene and propylene) but also prolong the catalyst lifetime by ∼3.7-fold in the methanol-to-olefin conversion. Structured illumination microscopy, *in situ* ultraviolet−visible spectroscopy, and online mass spectrometry elucidate the spatiotemporal distribution and evolution of the naphthalenic species during the precoking and steaming processes. This one-stone-two-birds strategy is applicable to a commercial SAPO-34 catalyst containing a binder, demonstrating its bright prospect in the methanol-to-olefin industry.

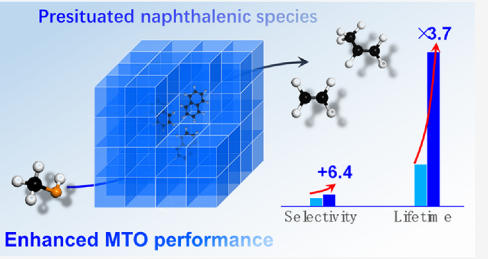

INTRODUCTION

With the shortage of oil resources, sustainable routes to produce lower olefins (ethylene and propylene) are highly desired, and thus, the methanol-to-olefin (MTO) reaction over microporous solid acids has attracted extensive attention from both the academic and industrial world.[1−7] SAPO-34 with small eight-membered ring pores and suitable acidity exhibits high olefin selectivity in the MTO conversion and has been utilized as the main part of a commercial MTO catalyst. However, rapid deactivation due to coke deposition is encountered, and thus, continuous regeneration of the catalyst is employed in real MTO operation.[8−10] The success of MTO relies on the process efficiency and economy, which largely depend on the product distribution and catalyst cost. In the past decade, extensive efforts have been devoted to prolong the single-pass catalyst lifetime and to promote the lower olefin selectivity, especially ethylene selectivity, over SAPO-34 catalysts to promote the process efficiency and economy. However, it is very difficult and challenging to achieve both goals simultaneously with a simple and feasible strategy.

The dual-cycle mechanism containing two competing cycles, *i.e.*, olefin- and aromatic-based cycles, is now well-understood and can be utilized to control the product distribution and catalyst lifetime in the MTO reaction. Ethylene is exclusively generated from the aromatic-based cycle, while propylene can be produced from both of the two cycles.[11,12] Accordingly, zeolite catalysts consisting of a suitable cage with a sufficient size to accommodate and confine the active hydrocarbon pool species are highly desired for proceeding the MTO conversion with high olefin selectivity. The Davis group[13−15] and the Corma group[16−18] investigated the light olefin selectivity−zeolite structure relationship independently from each other, and a zeolite structural indicator for low olefin selectivity during the MTO conversion has been established. Apart from the zeolite topology, adjusting the zeolite acidity,[19] reaction conditions,[19] and feed composition,[20−23] the product distribution in MTO conversion can be tuned in a certain range. Meanwhile, for the specific SAPO-34 catalysts, the aromatic-based cycle is the dominant mechanism in MTO conversion on the samples with either high or low acid density. It implies the possibility of promoting the ethylene selectivity without compromising propylene selectivity via the promotion of the aromatic-based cycle. Indeed, the strategy of precoking within SAPO-34 crystals through methanol[24] or *n*-butene[25] conversion at high temperatures, or through the partial regeneration of the used SAPO-34 catalyst,[8] to promote the ethylene selectivity, has been reported. On the other hand, the Zn-modified SAPO-34 catalyst can facilitate aromatic formation, thus promoting the ethylene selectivity.[26,27] Very recently, Liu and coworkers found that the naphthalenic

Received: October 3, 2022
Published: October 28, 2022

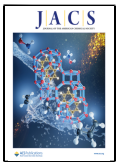

https://doi.org/10.1021/jacs.2c10495
J. Am. Chem. Soc. 2022, 144, 21408−21416

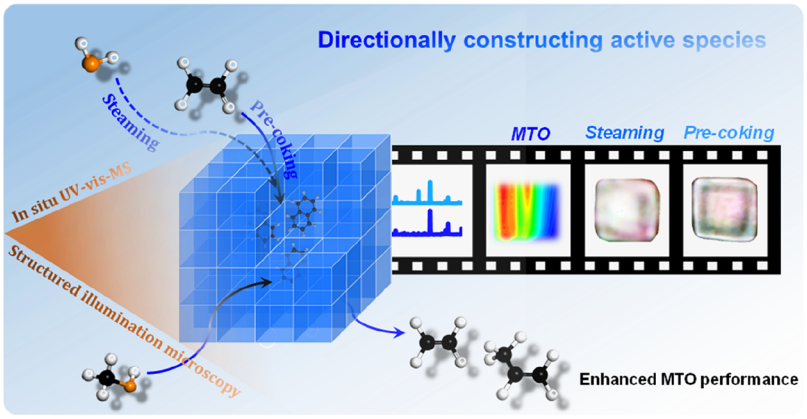

Figure 1. Schematic illustrations of directional construction of active naphthalenic species within the SAPO-34 catalyst.

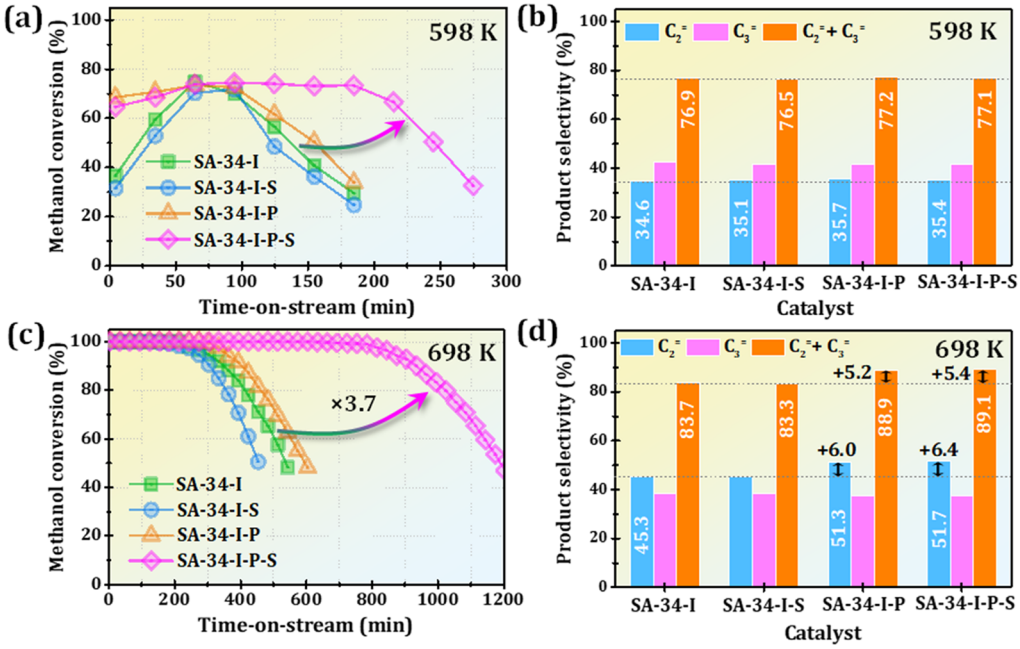

Figure 2. Time-dependent methanol conversion during the MTO reaction over different SAPO-34 catalysts at 598 (a) and 698 K (c) with a WHSV of 1.0 h^{-1} and the corresponding selectivity to ethylene and propylene recorded at TOS = 65 min (b,d). Precoking conditions: T = 698 K, $p(C_2H_4)$ = 50.0 kPa, F = 20 mL/min, and precoking time = 5 min. Steaming conditions: T = 698 K, WHSV = 1.0 h^{-1}, and steaming time = 5.0 h.

species originated from the cracking of deactivating coke compounds within the SAPO-34 crystals could also promote the ethylene selectivity.[28] Although these approaches can produce active naphthalenic species favoring ethylene formation within the cages of SAPO-34, a rapid catalyst deactivation in the MTO conversion is insurmountable. To prolong the catalyst lifetime by hindering the coke formation, numerous approaches like decreasing the crystal size,[29−33] reducing the acid density,[19,34] controlling the acid distribution,[35,36] introducing secondary large pores,[33,37−39] and cofeeding of water and/or H_2 in the reaction system[40−43] have been successfully developed. Meanwhile, for the specific zeolite catalyst, *e.g.*, SAPO-34 zeolite, the selectivity to lower olefins is not easy to alter via the aforementioned approaches simultaneously. There still appears a trade-off between ethylene selectivity and catalyst lifetime in MTO conversion over the specific SAPO-34 catalysts, and a feasible strategy to address both issues is challenging although it is extremely important in the MTO industry.

Herein, we develop a strategy combining precoking and steaming to directionally construct the active naphthalenic species within the crystal center of a SAPO-34 catalyst, which can significantly promote the lower olefin selectivity and catalyst lifetime in the MTO conversion at the same time. As elucidated by structured illumination microscopy (SIM), *in situ* UV−visible (UV−vis) spectroscopy, and online mass spectrometry (MS) (Figure 1), the naphthalenic species favoring ethylene formation can be formed at both the crystal rim and center by ethylene precoking. Subsequently, the naphthalenic species at the crystal rim can be efficiently cracked and eliminated via steaming, while those in the crystal center were well-retained. This rationally leads to a more efficient utilization of the catalyst crystals and suppresses the accumulation of coke compounds at the crystal rim, thus prolonging the catalyst lifetime. The simple and feasible strategy is readily applicable for commercial MTO catalysts containing a binder and therefore shows great prospects for industrial application.

https://doi.org/10.1021/jacs.2c10495
J. Am. Chem. Soc. 2022, 144, 21408−21416

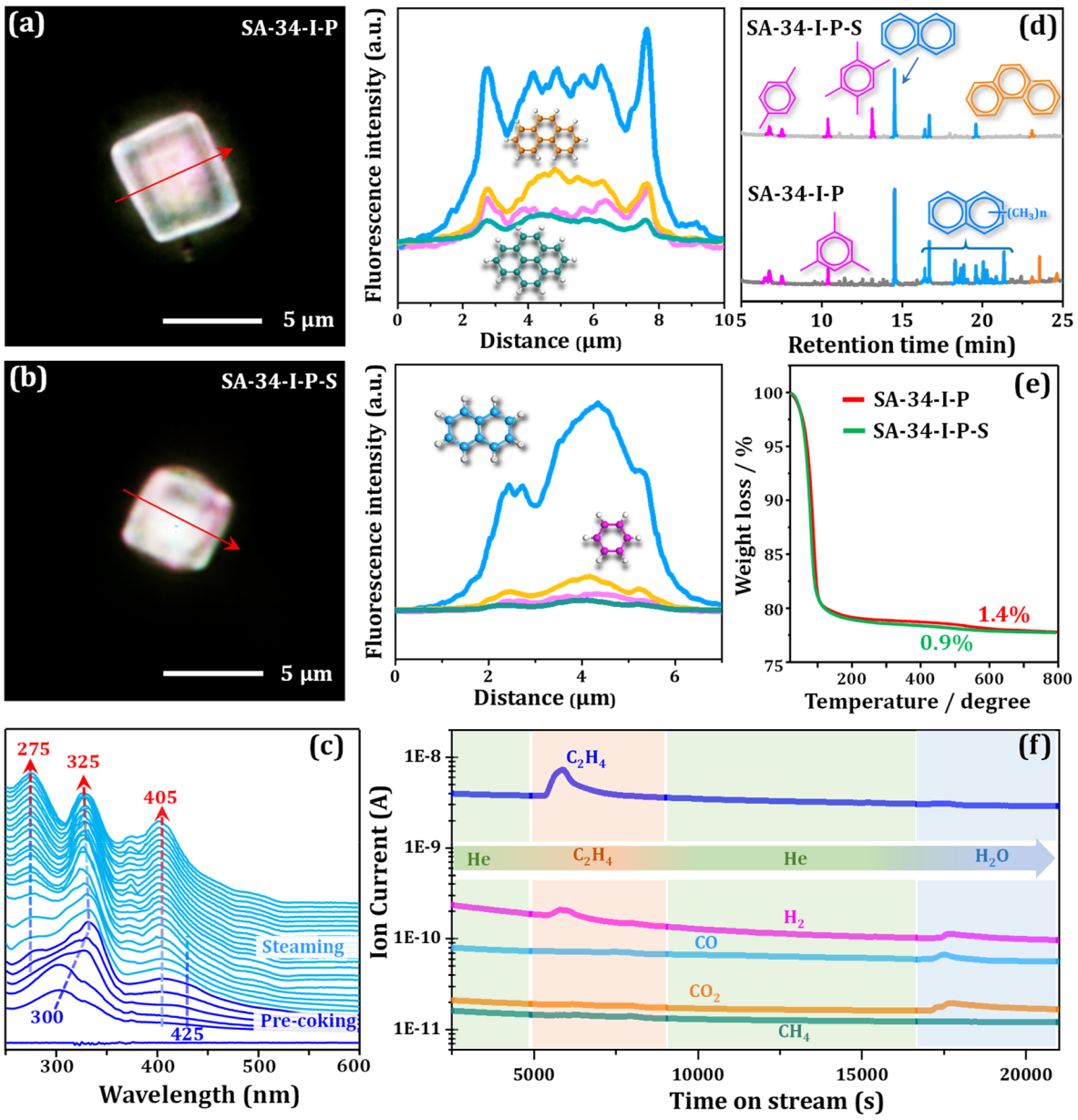

Figure 3. Spatiotemporal distribution of carbonaceous species obtained from SIM in SA-34-I-P (a) and SA-34-I-P-S (b) samples. The corresponding fluorescence intensities along the selected lines are also given on the right. The SIM pictures show the fluorescence originating from the overlap of four curves with different laser excitations of 405 (detection at 435−485 nm, pink curve), 488 (detection at 500−545 nm, blue curve), 561 (detection at 570−640 nm, orange curve), and 640 nm (detection at 663−738 nm, green curve). The images were taken in the middle plane of the zeolite crystal. (c) *In situ* UV−vis spectra recorded over the SA-34-I catalyst during the precoking and steaming processes at 698 K. (d) GC−MS chromatograms of organic extracts from SA-34-I-P and SA-34-I-P-S catalysts. (e) Coke amounts over SA-34-I-P and SA-34-I-P-S samples. (f) Online MS monitoring of C_2H_4, H_2, CO, CO_2, and CH_4 during the precoking and steaming processes over the SA-34-I catalyst at 698 K.

RESULTS AND DISCUSSION

Impacts of Precoking and Steaming on Product Distribution and Catalyst Lifetime. As is known,[24,28] naphthalenic species confined within the cages of the SAPO-34 catalyst can efficiently promote ethylene selectivity in MTO conversion. Our previous report revealed that naphthalenic species could be rapidly formed as the dominant intermediates during ethylene conversion over H-SSZ-13 zeolite.[44] Herein, ethylene precoking was first utilized to obtain the naphthalenic species-rich SAPO-34 sample, and subsequently, steaming was employed to eliminate the naphthalenic species at the crystal rim. The effects of the treatment parameters, *i.e.*, precoking and steaming time, on MTO performance over a model SAPO-34 catalyst (named as SA-34-I, Figures S1 and S2), were first examined at 698 K (Figure S3−6). Under the optimized treatment conditions, *i.e.*, precoking of 5 min and steaming of 5 h, the olefin selectivity and catalyst lifetime over different SAPO-34 samples were compared (Figure 2). At a low reaction temperature of 598 K, an obvious induction period of the MTO conversion occurs over the parent SA-34-I catalyst but can be greatly shortened over the precoked sample (named as SA-34-I-P) (Figure 2a). It indicates that the presituated aromatics species originated from ethylene precoking (*vide infra*) can efficiently promote MTO conversion. Owing to the good hydrothermal stability, the physicochemical properties of SA-34-I are preserved well after steaming treatment (Table

https://doi.org/10.1021/jacs.2c10495
J. Am. Chem. Soc. 2022, 144, 21408−21416

S1), and no obvious changes in MTO performance can be observed on the steamed sample (named as SA-34-I-S). Through the combination of precoking and subsequent steaming, a significant prolongation of the catalyst lifetime (with methanol conversion of ~70%) can be achieved, with the ethylene selectivity and the total selectivity to ethylene and propylene nearly unchanged (Figure 2b). In contrast, at a high temperature (698 K) with a complete methanol conversion, a significant improvement in ethylene selectivity (by ~6.0%) can be achieved over SA-34-I-P in comparison with the parent SA-34-I (Figure 2d). That is, precoking is an efficient strategy to promote the ethylene selectivity via the naphthalenic-based cycle at a high reaction temperature (*vide infra*), in line with the previous reports.[25,28] Analogous to the subcomplete conversion results, a significant improvement in the catalyst lifetime by 3.7-fold can be achieved over the SA-34-I-P-S at nearly full methanol conversion (>99%) in comparison with the parent SA-34-I (Figure 2c). Simultaneously, a significant increase in ethylene selectivity (from 45.3 to 51.3%) and total selectivity to ethylene and propylene (from 83.7 to 89.1%) can be achieved (Figure 2d). Overall, a combined strategy of precoking and steaming is effective for promoting both a lower olefin selectivity and catalyst lifetime in the MTO reaction over SAPO-34 catalysts.

Water cofeeding is frequently applied in MTO conversion to promote olefin selectivity or to prolong the catalyst lifetime. The olefin selectivity and catalyst stability of SA-34-I during MTO conversion with water cofeeding were evaluated for comparison. As shown in Figures S7 and S8, the catalyst lifetime can be prolonged by 2.1-fold with cofeeding 20 vol % water, while the ethylene selectivity and the total selectivity to ethylene and propylene remain nearly unchanged. These results further confirm the effectiveness and uniqueness of the combined strategy of precoking and subsequent steaming developed in this study.

Furthermore, the feasible strategy was also expanded to H-ZSM-5 and even H-SSZ-13 zeolites for improving the MTO performance. As shown in Figure S9, in comparison with the fresh H-SSZ-13-F and H-ZSM-5-F catalysts, a significant prolongation of the catalyst lifetime and the enhancement of the lower olefin selectivity could be achieved over the post-treated samples (named H-ZSM-5-P-S and H-SSZ-13-P-S). Furthermore, a partial dealumination occurred over the steamed H-SSZ-13 and H-ZSM-5 catalysts (Figure S9e,f), which could lead to the decrease of the Brønsted acid density, thus causing an obvious enhancement of the catalyst lifetime, while the ethylene selectivity and the total selectivity to ethylene and propylene remain nearly unchanged. These results confirm the effectiveness and uniqueness of the combined strategy of precoking and subsequent steaming developed in this study again.

Directional Construction of Active Naphthalenic Species. To clarify the nature and the spatiotemporal distribution of organic species formed during the precoking and steaming processes, high-resolution SIM was first applied. According to previous studies,[25,28,45−47] the benzene- (B^+), naphthalene- (N^+), phenanthrene- (PH^+), and pyrene-based (PYR^+) carbenium ions will give UV−vis bands at approximately 390, 480, 560, and 640 nm, respectively. Meanwhile, the corresponding emission wavelengths should be in the range of 480−490, 500−520, 620−630, and 670−700 nm, respectively. The excitation and emission wavelengths of the aromatic-based carbenium ions are fully covered in the present SIM measurements. As shown in Figure 3a and Figure S10, N^+ carbenium ions are already formed and appear as the dominant organic species at the crystal center and rim after precoking for 5 min. It has been reported that N^+ can serve as the active hydrocarbon pool species and favor ethylene formation in MTO conversion.[28] Consequently, an increase remarkable in the ethylene selectivity can be achieved over the SA-34-I-P catalyst (Figure 2d). After steaming at 698 K for 5 h, the relative fluorescence intensity of N^+ at the crystal rim declines sharply, hinting to their elimination by steaming. In contrast, the N^+ at the crystal center can be well-retained after steaming (Figure 3b and Figure S10). It reveals that the naphthalenic species have been successfully presituated at the crystal center after precoking and subsequent steaming.

The evolution of organic species formed during the precoking and steaming processes was further investigated by *in situ* UV−vis spectroscopy. As shown in Figure 3c, monoenylic carbenium ions and/or polyalkylaromatics (bands at ~300 nm)[48,49] are rapidly formed upon the introduction of ethylene and then gradually transferred to dienylic carbenium ions (325 nm)[50] and polycyclic aromatics with two and three condensed aromatic rings (405−425 nm).[51,52] Upon steaming, a gradual decrease of the bands at ~425 nm assigned to phenanthrenes or naphthalenes with more alkyl groups occurs. Simultaneously, a gradual increase of the band at 275 nm owing to polyalkylaromatics can be observed. This is well-supported by the GC−MS results (Figure 3d), where the amount of polymethylnaphthalenes and phenanthrenes occluded in the SA-34-I-P catalyst decreases distinctly with steaming, while that of polymethylbenzenes increases instead. According to the previous report,[53] this should be due to the cracking of phenanthrenes and/or naphthalenes during steaming, as phenanthrenes can be gradually transformed into naphthalenes, benzenes, and finally into CO and H_2. The composition of possible flue gas (including H_2, CO, CO_2, and CH_4) generated during the precoking and steaming processes was online monitored by MS. As shown in Figure 3f, H_2 is observed as the dominant small-molecule byproduct during the precoking process, revealing the occurrence of ethylene oligomerization, cyclization, and hydrogen transfer. Meanwhile, in the steaming process, H_2 and CO appear as the main gaseous products, indicating the occurrence of steam cracking.[28] Simultaneously, trace CO_2 appears in the gas phase due to the water-gas shift reaction.[53]

The aforementioned results clarify the directional construction of active naphthalenic species within the crystal center of SAPO-34 catalysts. As illustrated in Figure 4, the naphthalenes favoring ethylene formation in the MTO conversion can be formed and concentrated at both the crystal rim and center through ethylene precoking. On the other hand, owing to the steric hindrance, the naphthalenes at the crystal rim are easily accessible by water molecules and therefore cracked, while those deposited at the crystal center are highly stable and well-retained during steaming.[28] Consequently, only a slight decrease in the overall coke content occurs with further extension of steaming (Figure S11).

Mechanistic Interpretation for the Improvement in MTO Performance. The polymethyl aromatics confined within the cages of SAPO-34 may serve as the active hydrocarbon pool species to react with methanol molecules and trigger the MTO conversion.[24,54,55] Hence, the induction

https://doi.org/10.1021/jacs.2c10495
J. Am. Chem. Soc. 2022, 144, 21408−21416

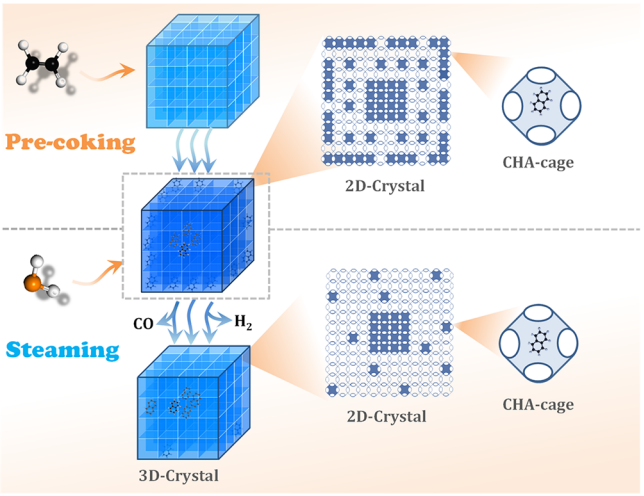

Figure 4. Schematic diagrams of the directional construction of active hydrocarbon pool species within SAPO-34 crystals.

period of MTO conversion at a low reaction temperature of 598 K is significantly shortened over the SA-34-I-P with the presituated aromatics (Figure 2a). However, no visible changes in ethylene selectivity occur over SA-34-I-P. With an increasing reaction temperature up to 698 K, however, a significant increase in ethylene selectivity can be achieved (Figure 2d). This is in line with the previous theoretical simulations that the methylated naphthalenes cannot serve as the active hydrocarbon pool species for ethylene formation at a low reaction temperature of 598 K,[56] while they can at a high temperature of 698 K.[28] On the other hand, the aromatics confined within the SAPO-34 crystals will hinder the intracrystalline self-diffusion of ethylene and propylene,[57,58] and naphthalenes will cause a more severe diffusion limitation of larger propylene than ethylene.[28] As a result, a remarkable improvement in ethylene selectivity can be achieved over SA-34-I-P and SA-34-I-P-S catalysts with the presituated naphthalenes owing to the common function in the above both sides (Figure 2c).

The acid density and pore characteristics of zeolite catalysts have important impacts on the catalyst stability during the MTO conversion. The physicochemical properties of SA-34-I zeolite before and after precoking and/or steaming were studied. The XRD patterns in Figure S12 indicate that the primary CHA structure can be well-preserved upon precoking and/or steaming. After precoking, noticeable decreases in the BET surface area, acid density, and microporous volume occur due to the formation of aromatics. Meanwhile, through steaming, the textural properties of SA-34-I and SA-34-I-P are well-maintained (Figure 5a, Figures S13−16, and Table S1); thus, the improvement in the MTO performance over SA-34-I-P-S from acid density variation or mesoporosity formation can be excluded in the present study. This is in line with the recent reports,[41] *i.e.*, steaming treatment can neither cause dealumination nor create mesopores in SAPO-34. Therefore, the essential reason for the improvement in MTO performance of SA-34-I-P-S requires further identification.

The structural and chemical characteristics of SAPO-34 samples may be inhomogeneous when steaming is done in a packed bed due to the diffusion effect. To reduce the diffusion effect to the most extent, we also employed the precoking and steaming treatments in an open quartz boat within a quartz tube. As shown in Figure S17, the zeolite samples in an open quartz boat within the glass tube could be more homogeneously exposed to water vapor during the steaming process.

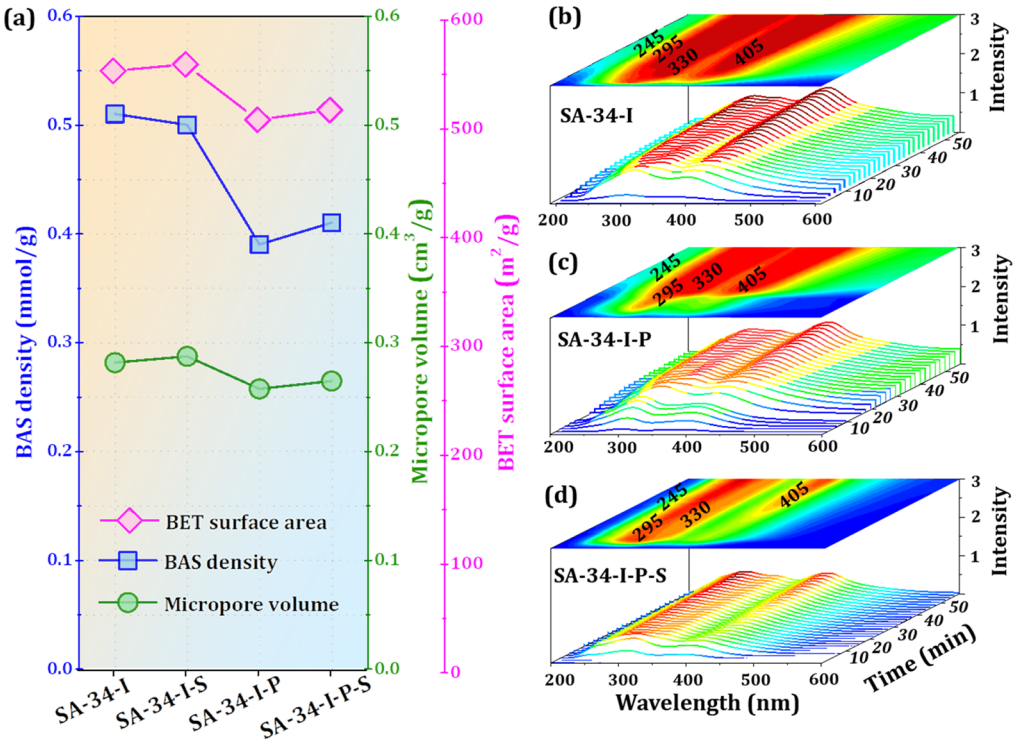

Figure 5. (a) Number of accessible Brønsted acid sites, micropore volume, and BET surface area of the SA-34-I catalyst before and after various treatments. *In situ* UV−vis spectra of MTO conversion over SA-34-I. (b) SA-34-I-P (c) and SA-34-I-P-S (d) catalysts recorded at 698 K with a TOS of 50 min.

https://doi.org/10.1021/jacs.2c10495
J. Am. Chem. Soc. 2022, 144, 21408−21416

After steaming, the structural characteristics and the catalytic performance of SA-34-I-P-S samples prepared in two different methods are compared and shown in Figure S18. Clearly, no obvious changes of the ^{27}Al, ^{31}P, and ^{29}Si MAS NMR spectra occur over SA-34-I-P-S samples obtained via the two different methods. Additionally, the two samples also exhibit the remarkable MTO activity, and an obvious enhancement of the catalyst lifetime by 3.5−3.7-fold could be achieved (Figure S18d). Simultaneously, a significant increase in ethylene selectivity by 5.9−6.4% and total selectivity to ethylene and propylene (from 83.7 to ∼89%) can be achieved (Figure S18e). These results reveal that the treatment process of steaming has no distinct effect on the structural characteristics and the catalytic performance of the SAPO-34 zeolite sample in the present study. On the other side, these results also indicate that the present strategy could be easily reproducible.

Recently, Beale and colleagues revealed that polyenes might be the crucial intermediates toward the formation of polycyclic aromatics, which were related to the catalyst deactivation.[7] The steric constraint of small zeolite cavities/channels can inhibit the intramolecular/intermolecular cyclization of polyenes, thus prolonging the catalyst lifetime. Therefore, it is supposed that the intramolecular or intermolecular cyclization of polyenes might be inhibited owing to the steric effect of the presituated naphthalenic species within SAPO-34 crystals. To get deeper insight into this hypothesis, *in situ* UV−vis spectroscopy was employed to monitor the nature of organic intermediates formed during MTO conversion over different SAPO-34 catalysts. As shown in Figure 5b,c, the amounts of small polyenes like dienes and dienylic cations over the SA-34-I-P catalyst, as reflected by the intensities of the UV−vis bands at 245 and 330 nm,[59] respectively, decline obviously in comparison with the parent SA-34-I catalyst. Simultaneously, a slight decrease of the intensities of neutral polyalkylaromatics (295 nm) and polycyclic aromatics with two or three condensed aromatic rings (∼405 nm) occurs.[59] It indicates that the cyclization of polyene to aromatics within SAPO-34 crystals can be suppressed by the presence of naphthalenic species, which is also supported by the thermogravimetric analyses (Figure S19), where less coke species are detected with the deactivated SA-34-I-P catalyst. Generally, postponing the accumulation of polycyclic aromatics can prolong the catalyst lifetime, but it is not the case here (Figure 2a,c). The naphthalenic species deposited at the crystal rim can accelerate MTO conversion, causing the accumulation of polycyclic aromatics at the crystal rim and accordingly reducing the accessibility of methanol or olefins to the Brønsted acid sites distributed in SAPO-34 crystals. This is supported by the ^{1}H MAS NMR results, where the Brønsted acid sites can be detected over the deactivated SA-34-I-P catalyst, but most of them are inaccessible by ammonia probe molecules (Figure S20). Meanwhile, for the SA-34-I-P-S catalyst, the elimination of the naphthalenic species deposited at the crystal rim can significantly enhance the diffusion of methanol inside the crystals, resulting in the more efficient utilization of the catalyst crystals and suppressing the accumulation of coke compounds at the crystal rim. On the other hand, the steric effect of the presituated naphthalenic species at the crystal center can hinder the rapid accumulation of polycyclic aromatics. Accordingly, the band intensities at ∼405 nm assigned to polycyclic aromatics decline significantly over the SA-34-I-P-S catalyst (Figure 5d), and a much longer catalyst lifetime is achieved (Figure 2c).

Industrial Prospect of the New Strategy. Long-term stability is an important metric for an industrial MTO catalyst, as the continuous regeneration in a fluidized bed reactor is required in real operation. To determine the industrial feasibility of the strategy developed in the present study, the MTO activity and the framework structure of SA-34-I and SA-34-I-P-S catalysts were compared through 20 regeneration cycles. As shown in Figures S21 and 22, no degradation in MTO performance, including both olefin selectivity and single-pass catalyst lifetime, can be observed for the SA-34-I-P-S catalyst after 20 cycles, confirming the feasibility and reproducibility of this new strategy. Some difference in the zeolite framework can be observed between SA-34-I and SA-34-I-P-S catalysts after 20 cycles. Compared with the SA-34-I-P-S catalyst, a slight decline in the intensity of XRD patterns appears for SA-34-I, indicating partial framework damage after the reaction. This is also supported by ^{1}H MAS NMR results, where the signal of the silanol group (δ_{1H} = 1.8 ppm), attributed to the breakage of bridge hydroxyl groups, appears over the SA-34-I catalyst, which is absent over the SA-34-I-P-S catalyst (Figure S23). Interestingly, the presituated naphthalenic species within SAPO-34 crystals can effectively protect the zeolite framework against hydrolysis. Overall, these results definitely demonstrate that the present strategy can promote the MTO performance of the SAPO-34 catalyst in terms of olefin selectivity, single-pass catalyst lifetime, and long-term stability, deriving a more efficient MTO process.

Finally, the strategy of precoking and subsequent steaming is applied to a structured commercial MTO catalyst containing a binder (named as SA-34-II) to directly test its industrial prospect. As shown in Figure 6, an improvement in MTO

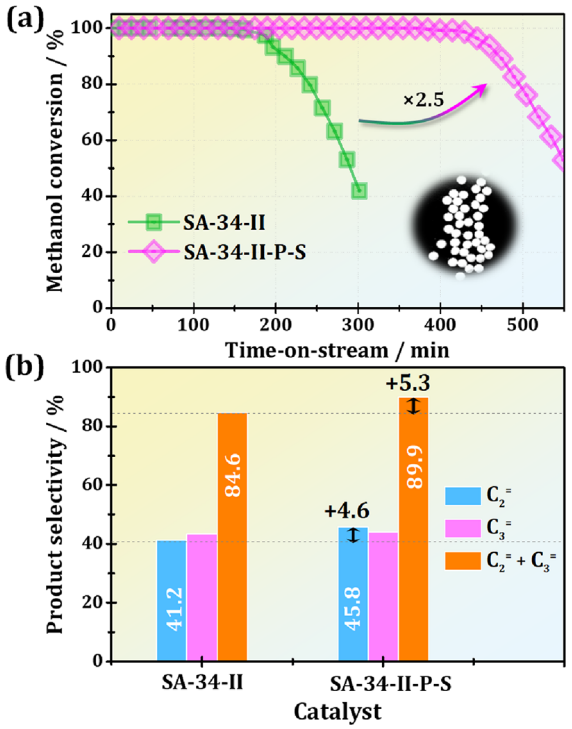

Figure 6. (a) Time-dependent methanol conversion over the commercial SA-34-II catalyst before and after treatments (precoking of 5 min and subsequent steaming of 5 h) during the MTO conversion at 698 K with a WHSV of 1.0 h^{-1} and (b) corresponding selectivity of ethylene and propylene recorded at TOS = 100 min.

https://doi.org/10.1021/jacs.2c10495
J. Am. Chem. Soc. 2022, 144, 21408−21416

performance can be achieved by employing such a strategy. In comparison with the parent SA-34-II catalyst, a significant prolongation of the catalyst lifetime by 2.5-fold can be achieved over the SA-34-II-P-S catalyst at 698 K (Figure 6a). Simultaneously, the ethylene selectivity can be promoted by 4.6% over the SA-34-II-P-S catalyst, and the high total selectivity to ethylene and propylene can reach up to ~90.0% (Figure 6b). These results reveal that the strategy developed herein is readily applicable to commercial MTO catalysts and shows great prospects in the MTO industry.

CONCLUSIONS

A feasible strategy combining precoking and subsequent steaming has been developed to directionally construct the active naphthalenic species within the crystal center of the SAPO-34 catalyst, which can promote the olefin selectivity and prolong the catalyst lifetime in the MTO conversion at the same time. Complementary approaches including SIM, *in situ* UV−vis, online MS, and GC−MS identify the spatiotemporal distribution and evolution of the carbonaceous species formed over SAPO-34 zeolite during the precoking and steaming processes. The naphthalenes favoring ethylene formation in the MTO conversion can be formed and concentrated at both the crystal rim and center by ethylene precoking. On the other hand, owing to the steric hindrance effect, the naphthalenes at the crystal rim are easily accessible by water molecules and cracked at high temperatures, while those deposited at the crystal center are highly stable and well-retained after steaming treatment. It rationally results in more efficient utilization of SAPO-34 crystals and suppresses the accumulation of coke compounds at the crystal rim, thus prolonging the catalyst lifetime. This feasible strategy is readily applicable to a commercial MTO catalyst containing a binder and therefore shows bright prospects in the current MTO industry.

ASSOCIATED CONTENT

Supporting Information

The Supporting Information is available free of charge at https://pubs.acs.org/doi/10.1021/jacs.2c10495.

Materials and characterization, catalytic study, solid-state NMR measurements, and additional results including *in situ* UV−vis measurements and more catalytic data (PDF)

AUTHOR INFORMATION

Corresponding Authors

Weili Dai − *School of Materials Science and Engineering, Nankai University, Tianjin 300350, P.R. China;* orcid.org/0000-0001-5752-0662; Email: weilidai@nankai.edu.cn

Landong Li − *School of Materials Science and Engineering, Nankai University, Tianjin 300350, P.R. China; Key Laboratory of Advanced Energy Materials Chemistry of the Ministry of Education, College of Chemistry, Nankai University, Tianjin 300071, P.R. China;* orcid.org/0000-0003-0998-4061; Email: lild@nankai.edu.cn

Authors

Chang Wang − *School of Materials Science and Engineering, Nankai University, Tianjin 300350, P.R. China*

Liu Yang − *School of Materials Science and Engineering, Nankai University, Tianjin 300350, P.R. China*

Mingbin Gao − *Dalian Institute of Chemical Physics, Chinese Academy of Sciences, Dalian 116023, P.R. China;* orcid.org/0000-0002-7143-2658

Xue Shao − *School of Materials Science and Engineering, Nankai University, Tianjin 300350, P.R. China*

Guangjun Wu − *School of Materials Science and Engineering, Nankai University, Tianjin 300350, P.R. China;* orcid.org/0000-0003-2633-5311

Naijia Guan − *School of Materials Science and Engineering, Nankai University, Tianjin 300350, P.R. China*

Zhaochao Xu − *Dalian Institute of Chemical Physics, Chinese Academy of Sciences, Dalian 116023, P.R. China;* orcid.org/0000-0002-2491-8938

Mao Ye − *Dalian Institute of Chemical Physics, Chinese Academy of Sciences, Dalian 116023, P.R. China;* orcid.org/0000-0002-7078-2402

Complete contact information is available at: https://pubs.acs.org/10.1021/jacs.2c10495

Notes

The authors declare no competing financial interest.

ACKNOWLEDGMENTS

This work was supported by the National Natural Science Foundation of China (21972069 and 22121005) and the Fundamental Research Funds for the Central Universities (Nankai University).

REFERENCES

(1) Olsbye, U.; Svelle, S.; Bjørgen, M.; Beato, P.; Janssens, T. V. W.; Joensen, F.; Bordiga, S.; Lillerud, K. P. Conversion of Methanol to Hydrocarbons: How Zeolite Cavity and Pore Size Controls Product Electivity. *Angew. Chem., Int. Ed.* **2021**, *51*, 5810−5831.

(2) Van Speybroeck, V.; De Wispelaere, K.; Van der Mynsbrugge, J.; Vandichel, M.; Hemelsoet, K.; Waroquier, M. First Principle Chemical Kinetics in Zeolites: The Methanol-to-Olefin Process as a Case Study. *Chem. Soc. Rev.* **2014**, *43*, 7326−7357.

(3) Olsbye, U.; Svelle, S.; Lillerud, K. P.; Wei, Z. H.; Chen, Y. Y.; Li, J. F.; Wang, J. G.; Fan, W. B. The Formation and Degradation of Active Species during Methanol Conversion over Protonated Zeotype Catalysts. *Chem. Soc. Rev.* **2015**, *44*, 7155−7176.

(4) Yarulina, I.; Chowdhury, A. D.; Meirer, F.; Weckhuysen, B. M.; Gascon, J. Recent Trends and Fundamental Insights in the Methanol-to-Hydrocarbons Process. *Nat. Catal.* **2018**, *1*, 398−411.

(5) Yarulina, I.; De Wispelaere, K.; Bailleul, S.; Goetze, J.; Radersma, M.; Abou-Hamad, E.; Vollmer, I.; Goesten, M.; Mezari, B.; Hensen, E. J. M.; Martínez-Espín, J. S.; Morten, M.; Mitchell, S.; Perez-Ramirez, J.; Olsbye, U.; Weckhuysen, B. M.; Van Speybroeck, V.; Kapteijn, F.; Gascon, J. Structure-Performance Descriptors and the Role of Lewis Acidity in the Methanol-to-Propylene Process. *Nat. Catal.* **2018**, *10*, 804−812.

(6) Hwang, A.; Bhan, A. Deactivation of Zeolites and Zeotypes in Methanol-to-Hydrocarbons Catalysis: Mechanisms and Circumvention. *Acc. Chem. Res.* **2019**, *52*, 2647−2656.

(7) Lezcano-Gonzalez, I.; Campbell, E.; Hoffman, A. E. J.; Bocus, M.; Sazanovich, I. V.; Towrie, M.; Agote-Aran, M.; Gibson, E. K.; Greenaway, A.; De Wispelaere, K.; Van Speybroeck, V.; Beale, A. M. Insight into the Effects of Confined Hydrocarbon Species on the Lifetime of Methanol Conversion Catalysts. *Nat. Mater.* **2020**, *19*, 1081−1087.

(8) Tian, P.; Wei, Y.; Ye, M.; Liu, Z. Methanol to Olefins (MTO): From Fundamentals to Commercialization. *ACS Catal.* **2015**, *5*, 1922−1938.

(9) Yang, M.; Fan, D.; Wei, Y.; Tian, P.; Liu, Z. Recent Progress in Methanol-to-Olefins (MTO) Catalysts. *Adv. Mater.* **2019**, *31*, 1902181.

(10) Yang, L.; Wang, C.; Zhang, L.; Dai, W.; Chu, Y.; Xu, J.; Wu, G.; Gao, M.; Liu, W.; Xu, Z.; Wang, P.; Guan, N.; Dyballa, M.; Ye, M.; Deng, F.; Fan, W.; Li, L. Stabilizing the Framework of SAPO-34 Zeolite toward Long-Term Methanol-to-Olefins Conversion. *Nat. Commun.* **2021**, *12*, 4661.
(11) Svelle, S.; Joensen, F.; Nerlov, J.; Olsbye, U.; Lillerud, K.-P.; Kolboe, S.; Bjørgen, M. Conversion of Methanol into Hydrocarbons over Zeolite H-ZSM-5: Ethene Formation is Mechanistically Separated from the Formation of Higher Alkenes. *J. Am. Chem. Soc.* **2006**, *128*, 14770−14771.
(12) Bjørgen, M.; Svelle, S.; Joensen, F.; Nerlov, J.; Kolboe, S.; Bonino, F.; Palumbo, L.; Bordiga, S.; Olsbye, U. Conversion of Methanol to Hydrocarbons over Zeolite H-ZSM-5: on the Origin of the Olefinic Species. *J. Catal.* **2007**, *249*, 195−207.
(13) Bhawe, Y.; Moliner-Marin, M.; Lunn, J. D.; Liu, Y.; Malek, A.; Davis, M. Effect of Cage Size on the Selective Conversion of Methanol to Light Olefins. *ACS Catal.* **2012**, *2*, 2490−2495.
(14) Kang, J. H.; Walter, R.; Xie, D.; Davis, T.; Chen, C.-Y.; Davis, M. E.; Zones, S. I. Further Studies on How the Nature of Zeolite Cavities That Are Bounded by Small Pores Influences the Conversion of Methanol to Light Olefins. *ChemPhysChem* **2018**, *19*, 412−419.
(15) Kang, J. H.; Alshafei, F. H.; Zones, S. I.; Davis, M. E. Cage-Defining Ring: A Molecular Sieve Structural Indicator for Light Olefin Product Distribution from the Methanol-to-Olefins Reaction. *ACS Catal.* **2019**, *9*, 6012−6019.
(16) Li, C.; Paris, C.; Martínez-Triguero, J.; Boronat, M.; Moliner, M.; Corma, A. Synthesis of Reaction-Adapted Zeolites as Methanol-to-Olefins Catalysts with Mimics of Reaction Intermediates as Organic Structure-Directing Agents. *Nat. Catal.* **2018**, *1*, 547−554.
(17) Ferri, P.; Li, C.; Paris, C.; Vidal-Moya, A.; Moliner, M.; Boronat, M.; Corma, A. Chemical and Structural Parameter Connecting Cavity Architecture, Confined Hydrocarbon Pool Species, and MTO Product Selectivity in Small-Pore Cage-Based Zeolites. *ACS Catal.* **2019**, *9*, 11542−11551.
(18) Ferri, P.; Li, C.; Millán, R.; Martínez-Triguero, J.; Moliner, M.; Boronat, M.; Corma, A. Impact of Zeolite Framework Composition and Flexibility on Methanol-To-Olefins Selectivity: Confinement or Diffusion? *Angew. Chem., Int. Ed.* **2020**, *59*, 19708−19715.
(19) Dai, W.; Cao, G.; Yang, L.; Wu, G.; Dyballa, M.; Hunger, M.; Guan, N.; Li, L. Insights into the Catalytic Cycle and Activity of Methanol-to-Olefin Conversion over Low-Silica AlPO-34 Zeolites with Controllable Brønsted Acid Density. *Catal. Sci. Technol.* **2007**, *7*, 607−618.
(20) Martínez-Espin, J. S.; De Wispelaere, K.; Janssens, T. V. W.; Svelle, S.; Lillerud, K. P.; Beato, P.; Van Speybroeck, V.; Olsbye, U. Hydrogen Transfer Versus Methylation: on the Genesis of Aromatics Formation in the Methanol-to-Hydrocarbons Reaction over H-ZSM-5. *ACS Catal.* **2017**, *7*, 5773−5780.
(21) Khare, R.; Bhan, A. Mechanistic Studies of Methanol-to-Hydrocarbons Conversion on Diffusion-Free MFI Samples. *J. Catal.* **2019**, *329*, 218−228.
(22) Liu, Y.; Kirchberger, F. M.; Müller, S.; Eder, M.; Tonigold, M.; Sanchez-Sanchez, M.; Lercher, J. A. Critical Role of Formaldehyde During Methanol Conversion to Hydrocarbons. *Nat. Commun.* **2019**, *10*, 1462.
(23) Yang, L.; Yan, T.; Wang, C.; Dai, W.; Wu, G.; Hunger, M.; Fan, W.; Xie, Z.; Guan, N.; Li, L. Role of Acetaldehyde in the Roadmap from Initial Carbon-Carbon Bonds to Hydrocarbons during Methanol Conversion. *ACS Catal.* **2019**, *9*, 6491−6501.
(24) Song, W.; Fu, H.; Haw, J. F. Selective Synthesis of Methylnaphthalenes in HSAPO-34 Cages and their Function as Reaction Centers in Methanol-to-Olefin Catalysis. *J. Phys. Chem. B.* **2001**, *105*, 12839−12843.
(25) Zhou, J.; Zhou, Y.; Zhang, J.; Liu, Z.; Zhang, T.; He, Y.; Zheng, A.; Ye, M.; Wei, Y.; Liu, Z. Presituated "coke"-Determined Mechanistic Route for Ethene Formation in the Methanol-to-Olefins Process on SAPO-34 Catalyst. *J. Catal.* **2019**, *377*, 153−162.
(26) Zhong, J.; Han, J.; Wei, Y.; Xu, S.; He, Y.; Ye, M.; Zheng, Y.; Guo, X.; Song, C.; Liu, Z. Increasing the Selectivity to Ethylene in the MTO Reaction by Enhancing Diffusion Limitation in the Shell Layer of SAPO-34 Catalyst. *Chem. Commun.* **2018**, *54*, 3146−3149.
(27) Huang, H.; Wang, H.; Zhu, H.; Zhang, S.; Zhang, Q.; Li, C. Enhanced Ethene to Propene Ratio over Zn-Modified SAPO-34 Zeolites in Methanol-to-Olefin Reaction. *Catal. Sci. Technol.* **2019**, *9*, 2203−2210.
(28) Zhou, J.; Gao, M.; Zhang, J.; Liu, W.; Zhang, T.; Li, H.; Xu, Z.; Ye, M.; Liu, Z. Directed Transforming of Coke to Active Intermediates in Methanol-to-Olefins Catalyst to Boost Light Olefins Selectivity. *Nat. Commun.* **2021**, *12*, 17.
(29) Chen, D.; Moljord, K.; Fuglerud, T.; Holmen, A. The Effect of Crystal Size of SAPO-34 on the Selectivity and Deactivation of the MTO Reaction. *Microporous Mesoporous Mater.* **1999**, *29*, 191−203.
(30) Nishiyama, N.; Kawaguchi, M.; Hirota, Y.; Vu, D. V.; Egashira, Y.; Ueyama, K. Size Control of SAPO-34 Crystals and their Catalyst Lifetime in the Methanol-to-Olefin Reaction. *Appl. Catal., A* **2009**, *362*, 193−199.
(31) Sun, Q.; Ma, Y.; Wang, N.; Li, X.; Xi, D.; Xu, J.; Deng, F.; Yoon, K. B.; Oleynikov, P.; Terasaki, O.; Yu, J. High Performance Nanosheet-Like Silicoaluminophosphate Molecular Sieves: Synthesis, 3D EDT Structural Analysis and MTO Catalytic Studies. *J. Mater. Chem. A* **2014**, *2*, 17828−17839.
(32) Li, Z.; Martínez-Triguero, J.; Yu, J.; Corma, A. Conversion of Methanol to Olefins: Stabilization of Nanosized SAPO-34 by Hydrothermal Treatment. *J. Catal.* **2015**, *329*, 379−388.
(33) Zhong, J.; Han, J.; Wei, Y.; Tian, P.; Guo, X.; Song, C.; Liu, Z. Recent Advances of the Nano-Hierarchical SAPO-34 in the Methanol-to-Olefin (MTO) Reaction and Other Applications. *Catal. Sci. Technol.* **2017**, *7*, 4905−4923.
(34) Gao, B.; Yang, M.; Qiao, Y.; Li, J.; Xiang, X.; Wu, P.; Wei, Y.; Xu, S.; Tian, P.; Liu, Z. A Low-Temperature Approach to Synthesize Low-Silica SAPO-34 Nanocrystals and their Application in the Methanol-to-Olefins (MTO) Reaction. *Catal. Sci. Technol.* **2016**, *6*, 7569−7578.
(35) Martínez-Franco, R.; Li, Z.; Martínez-Triguero, J.; Moliner, M.; Corma, A. Improving the catalytic performance of SAPO-18 for Methanol-to-Olefins (MTO) by controlling the Si distribution and crystal size. *Catal. Sci. Technol.* **2016**, *6*, 2796−2806.
(36) Gallego, E. M.; Li, C.; Paris, C.; Martín, N.; Martínez-Triguero, J.; Boronat, M.; Moliner, M.; Corma, A. Making Nanosized CHA Zeolites with Controlled Al Distribution for Optimizing Methanol-to-Olefin Performance. *Chem. − Eur. J.* **2018**, *24*, 14631−14635.
(37) Sun, Q.; Wang, N.; Xi, D.; Yang, M.; Yu, J. Organosilane Surfactant-Directed Synthesis of Hierarchical Porous SAPO-34 Catalysts with Excellent MTO Performance. *Chem. Commun.* **2014**, *50*, 6502−6505.
(38) Xi, D.; Sun, Q.; Xu, J.; Cho, M.; Cho, H. S.; Asahina, S.; Li, Y.; Deng, F.; Terasaki, O.; Yu, J. *In situ* Growth-Etching Approach to the Preparation of Hierarchically Macroporous Zeolites with High MTO Catalytic Activity and Selectivity. *J. Mater. Chem. A* **2014**, *2*, 17994−18004.
(39) Liang, Y.; Gao, B.; Zhou, L.; Yang, X.; Lu, T.; Yao, H.; Su, Y. Rational Construction of Hierarchical SAPO-34 with Enhanced MTO Performance without an Additional Meso/Macropore Template. *J. Mater. Chem. A* **2021**, *9*, 1859−1867.
(40) Wu, X.; Anthony, R. G. Effect of Feed Composition on Methanol Conversion to Light Olefins over SAPO-34. *Appl. Catal., A* **2001**, *218*, 241−250.
(41) De Wispelaere, K.; Wondergem, C. S.; Ensing, B.; Hemelsoet, K.; Jan Meijer, E.; Weckhuysen, B. M.; Van Speybroeck, V.; Ruiz-Martínez, J. Insight into the Effect of Water on the Methanol-to-Olefins Conversion in H-SAPO-34 from Molecular Simulations and *in situ* Microspectroscopy. *ACS Catal.* **2016**, *6*, 1991−2002.
(42) Arora, S. S.; Nieskens, D. L. S.; Malek, A.; Bhan, A. Lifetime Improvement in Methanol-to-Olefins Catalysis over Chabazite Materials by High-Pressure H_2 co-Feeds. *Nat. Catal.* **2018**, *1*, 666−672.
(43) Zhao, X.; Li, J.; Tian, P.; Wang, L.; Li, X.; Lin, S.; Guo, X.; Liu, Z. Achieving a Superlong Lifetime in the Zeolite-Catalyzed MTO

Reaction under High Pressure: Synergistic Effect of Hydrogen and Water. *ACS Catal.* **2019**, *9*, 3017−3025.
(44) Dai, W.; Sun, X.; Tang, B.; Wu, G.; Li, L.; Guan, N.; Hunger, M. Verifying the Mechanism of the Ethene-to-Propene Conversion on Zeolite H-SSZ-13. *J. Catal.* **2014**, *314*, 10−20.
(45) Whiting, G. T.; Nikolopoulos, N.; Nikolopoulos, I.; Chowdhury, A. D.; Weckhuysen, B. M. Visualizing Pore Architecture and Molecular Transport Boundaries in Catalyst Bodies with Fluorescent Nanoprobes. *Nat. Chem.* **2019**, *11*, 23−31.
(46) Van Speybroeck, V.; Hemelsoet, K.; Wispelaere, K. D.; Qian, Q.; Van der Mynsbrugge, J.; De Sterck, B.; Weckhuysen, B. M.; Waroquier, M. Mechanistic Studies on Chabazite-Type Methanol-to-Olefin Catalysts: Insights from Time-Resolved UV/Vis Microspectroscopy Combined with Theoretical Simulations. *ChemCatChem* **2013**, *5*, 173−184.
(47) Gao, M.; Li, H.; Liu, W.; Xu, Z.; Peng, S.; Yang, M.; Ye, M.; Liu, Z. Imaging Spatiotemporal Evolution of Molecules and Active Sites in Zeolite Catalyst During Methanol-to-Olefins Reaction. *Nat. Commun.* **2020**, *11*, 3641.
(48) Deno, N. C.; Bollinger, J.; Friedman, N.; Hafer, K.; Hodge, J. D.; Houser, J. J. Carbonium ions. XIII. Ultraviolet Spectra and Thermodynamic Stabilities of Cycloalkenyl and Linear Alkenyl Cations. *J. Am. Chem. Soc.* **1963**, *85*, 2998−3000.
(49) Dai, W.; Wang, C.; Dyballa, M.; Wu, G.; Guan, N.; Li, L.; Xie, Z.; Hunger, M. Understanding the Early Stages of the Methanol-to-Olefin Conversion on H-SAPO-34. *ACS Catal.* **2015**, *5*, 317−326.
(50) Nagy, J. B.; Kiricsi, I.; Förster, H.; Tasi, G. Generation, Characterization and Transformation of Unsaturated Carbenium ions in Zeolites. *Chem. Rev.* **1999**, *99*, 2085−2114.
(51) Jiang, Y.; Huang, J.; Marthala, V. R. R.; Ooi, Y. S.; Weitkamp, J.; Hunger, M. *In situ* MAS NMR−UV/Vis Investigation of H-SAPO-34 Catalysts Partially Coked in the Methanol-to-Olefin Conversion under Continuous-Flow Conditions and of their Regeneration. *Microporous Mesoporous Mater.* **2007**, *105*, 132−139.
(52) Park, J. W.; Lee, J. Y.; Kim, K. S.; Hong, S. B.; Seo, G. Effects of Cage Shape and Size of 8-Membered Ring Molecular Sieves on their Deactivation in Methanol-to-Olefin (MTO) Reactions. *Appl. Catal., A* **2008**, *339*, 36−44.
(53) Wang, Q.; Li, Q.; Tsuboi, Y.; Zhang, Y.; Zhang, H.; Zhang, J. Decomposition of Pyrene by Steam Reforming: the Effects of Operational Conditions and Kinetics. *Fuel Process. Technol.* **2018**, *182*, 88−94.
(54) Song, W.; Haw, J. F.; Nicholas, J. B.; Heneghan, C. S. Methylbenzenes are the Organic Reaction Centers for Methanol-to-Olefin Catalysis on HSAPO-34. *J. Am. Chem. Soc.* **2000**, *122*, 10726−10727.
(55) Arstad, B.; Kolboe, S. The Reactivity of Molecules Trapped within the SAPO-34 Cavities in the Methanol-to-Hydrocarbons Reaction. *J. Am. Chem. Soc.* **2001**, *123*, 8137−8138.
(56) Hemelsoet, K.; Nollet, A.; Van Speybroeck, V.; Waroquier, M. Theoretical Simulations Elucidate the Role of Naphthalenic Species during Methanol Conversion within H-SAPO-34. *Chem. − Eur. J.* **2011**, *17*, 9083−9093.
(57) Dai, W.; Scheibe, M.; Li, L.; Guan, N.; Hunger, M. Effect of the Methanol-to-Olefin Conversion on the PFG NMR Self-Diffusivities of Ethane and Ethene in Large-Crystalline SAPO-34. *J. Phys. Chem. C* **2012**, *116*, 2469−2476.
(58) Cnudde, P.; Demuynck, R.; Vandenbrande, S.; Waroquier, M.; Sastre, G.; Speybroeck, V. V. Light Olefin Diffusion during the MTO Process on H-SAPO-34: A Complex Interplay of Molecular Factors. *J. Am. Chem. Soc.* **2020**, *142*, 6007−6017.
(59) Dai, W.; Wu, G.; Li, L.; Guan, N.; Hunger, M. Mechanisms of the Deactivation of SAPO-34 Materials with Different Crystal Sizes Applied as MTO Catalysts. *ACS Catal.* **2013**, *3*, 588−596.

https://doi.org/10.1021/jacs.2c10495
J. Am. Chem. Soc. 2022, 144, 21408−21416